Neural mechanism of attention modulation during non-movement decision-making

Shengnan Ai[1,2], **Jiamin Wu**[1,2*], **Qionghai Dai**[1,2,3*]

***For correspondence:**
qhdai@tsinghua.edu.cn (Q. D.);
wujiamin@tsinghua.edu.cn (W. J.)

[1]Department of Automation, Tsinghua University, Beijing, 100084, China; [2]Institute for Brain and Cognitive Sciences, Tsinghua University; Beijing 100084, China; [3]Beijing National Research Center for Information Science and Technology, Tsinghua University, Beijing 100084, China

Abstract Decision-making is a cognitive process, in which participants need to attend to relevant information and ignore the irrelevant information. To identify the attention mechanism in a non-movement decision-making process, we re-analyze local field potential signals from a task, in which subjects were instructed to attend to specific numbers. Given the important role of theta and broadband high gamma (BHG) oscillations in attentional processing (***Baird et al.*** (***2014***); ***Foster et al.*** (***2013***); ***Helfrich et al.*** (***2018***)). We examined theta-BHG coupling within and between dorsal posterior prefrontal cortex (dpPFC), dorsal lateral prefrontal cortex (dlPFC), medial prefrontal cortex (mPFC), and subthalamic nucleus (STN) as a function of attention states (attended or ignored). We found decreased phase-amplitude coupling (PAC) between theta and BHG during the attended trials, within each area and cross areas. Our results indicate that STN participated in attention processing for the first time, and the decreased PAC in STN and prefrontal regions between theta and BHG is a core electrophysiological mechanism that underlies selective attention allocation.

Introduction

Attention is a core internal state variable that governs the allocation of limited resources depending on the task demands in various cognitive processes. The attentional modulation has a hierarchical structure: goals at higher levels inform the focus of attention at lower levels (goal-directed top-down attention modulation), while stimulus at lower levels informs decisions regarding which information to attend to (stimulus-driven bottom-up attention modulation) (***Suzuki and Gottlieb*** (***2013***); ***Gregoriou et al.*** (***2014***); ***Buckley et al.*** (***2009***); ***Buschman and Kastner*** (***2015***); ***Foxe and Snyder*** (***2011***)).

Building on decades of functional neuroimaging research, two widespread cortical networks were characterized, including the dorsal attention network (DAN) and the salience network (SN) (***Dubey et al.*** (***2023***)***Corbetta and Shulman*** (***2002***)). The DAN is believed as neural basis of top-down attention modulation, located in frontal and posterior parietal cortex (PPC). And the SN is believed as neural basis of bottom-up attention modulation, located in temporal-parietal junction (TPJ) and inferior, middle and superior frontal cortex (***Seeley et al.*** (***2007***); ***Uddin*** (***2014***)). These two networks interact dynamically with each other during attentional processing (***Vossel et al.*** (***2005***)).

Besides advances in neuroimaging technologies, the ability to conduct high-density multi-channel electroencephalogram (EEG) and magnetoencephalography (MEG) have unprecedentedly progressed

our understanding of the physiology of human selective attention. Findings from neurophysiological studies indicated that theta and BHG activities held important roles in attentional modulation. Some studies in nonhuman primates have shown that selective attention decreases the coupling between the amplitude of gamma oscillations and the phase of theta oscillations in visual cortex (***Spyropoulos et al.*** (***2018***); ***Esghaei et al.*** (***2015***)). An EEG oscillation study in human revealed that theta power in midfrontal area is related to the attention selection during cognitive conflict processing (***Haciahmet et al.*** (***2021***)). A MEG study indicated stronger theta (3-7 Hz) responses in dorsolateral, ventral, and medial frontal regions during incongruent trials relative to congruent trials (***McDermott et al.*** (***2017***)). One Electrocorticography (ECoG) study found increases in high gamma (HG) power (70-250 Hz) compared to baseline over frontal, parietal, and visual areas. The high gamma power increases were modulated by the phase of the delta/theta (2-5 Hz) oscillation during attentional allocation in a visuospatial-cuing task (***Szczepanski et al.*** (***2014***)). Another iEEG study also found that theta power (4 Hz) mediated fluctuations in widespread cortical areas are behaviorally related to visual attention performance, and high-frequency band (HFB; 70-150 Hz) activity was nested in an ongoing 4 Hz oscillation (***Helfrich and Knight*** (***2016***)).

These attention-dependent changes in neurophysiology have so far mainly focused on cortical regions in the brain. It is unclear whether attention modulation mechanisms work in a similar way in subcortical areas. The STN is a small lens-shaped subcortical nucleus as a part of basal ganglia. It is traditionally considered a critical node in the cortico-basal ganglia-thalamus-cortico network, which composed of the direct pathway (cortex-striatum [Str]-substantia nigra [SNr]- internal globus pallidus [GPi]-thalamus), indirect pathway (cortex-Str-external globus pallidus [GPe]-STN-SNr/GPi-thalamus]), and hyper-direct pathway (cortex-STN-SNr/GPi-thalamus) (***Drummond and Chen*** (***2020***); ***Nambu et al.*** (***2002***); ***Eliasmith et al.*** (***2012***)). Given the location of the STN and its widespread connections with cortical and subcortical brain regions (***Taylor et al.*** (***2007***); ***Coxon et al.*** (***2012***); ***Forstmann et al.*** (***2012***); ***King et al.*** (***2011***)), the STN plays an important role in motor and non-motor cognitive processing (***Zavala et al.*** (***2018***); ***Wessel et al.*** (***2019***); ***Herz et al.*** (***2017***); ***Haynes and Haber*** (***2013***); ***Popov et al.*** (***2013***); ***Kühn et al.*** (***2005***)). We would like to know if STN also participates in attention regulations, and how the STN interacts with cortical regions during the attentional regulation process.

In the present study, we address these unanswered questions by examining theta-BHG phase-amplitude coupling within and cross regions located in three prefrontal regions and STN. We predicted that BHG activity, a proxy for local spiking activity or cortical excitability (***Ray and Maunsell*** (***2011***); ***Watson et al.*** (***2017***)), is modulated by theta activity. We hypothesized that the phase-amplitude coupling between theta band oscillations and BHG modulated by the attended or ignored brain states, and the modulation existed not only in one particular brain region, but cross regions of prefrontal cortex and STN, facilitating interregional information transfer (***Helfrich and Knight*** (***2016***); ***Helfrich et al.*** (***2018***)).

Results

We re-analyze electrophysiological data recorded in Parkinson's patients during a novel non-motor decision-making task that requires participants to decide whether to encode items into working memory (***Zavala et al.*** (***2017***)). Eighteen patients (16 males; 58.4+/-1.64 (mean SEM) years old) participated in the task. Local field potential (LFP) and neuronal spiking activity in the human STN and intracranial EEG (iEEG) activity from the PFC were captured. In our study, the LFP in the human STN, iEEG in dorsal posterior prefrontal cortex (dpPFC), dorsal lateral prefrontal cortex (dlPFC), and medial prefrontal cortex (mPFC) were used for analysis.

Behavior results

During each task block, a target shape (square or octagon) was first presented to participants. Then eight single-digit numbers were sequentially presented to participants, in which four of the numbers appeared within the target shape (target trials). Four target numbers and four distract

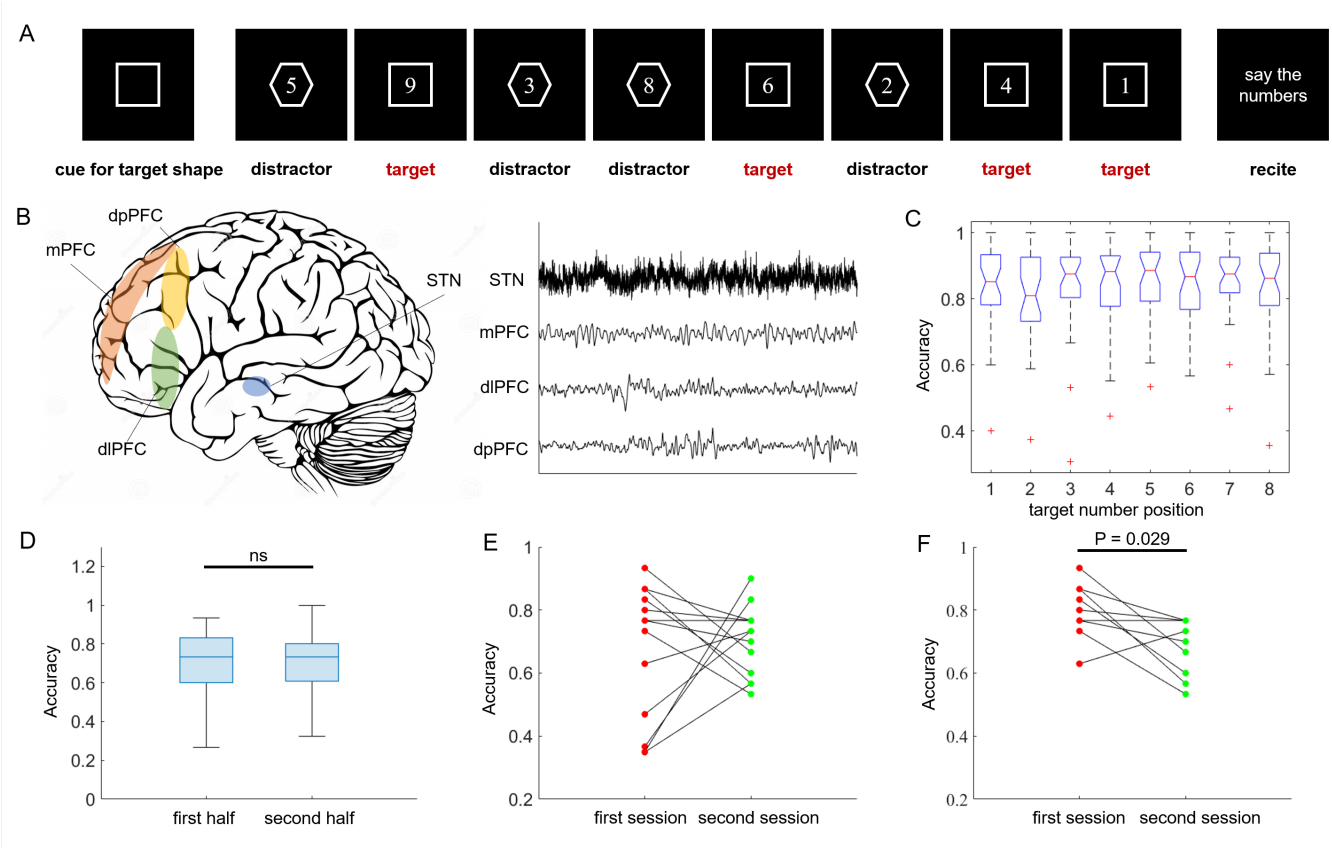

Figure 1. (A) non-motor decision making task. (B) Left panel, ECoG strips were placed over the medial, dorsal posterior, and dorsal lateral prefrontal cortex, respectively. Macroelectrodes were placed in STN. Right panel, a sample recording from one trial is shown for electrodes placed in each region. (C) Accuracy for target number placed in each sequential position. (D) Accuracy for target numbers in first and second half of one experimental session. (E) Accuracy for the first and second session of one participant. (F) Accuracy for the first and second session of one participant, after four participants were removed.

numbers were randomly interleaved. Participants were instructed only to attend to and memorize numbers presented within the target shape. At the end of each block, participants vocalized the numbers they remembered.

We first investigated if the position of the target number in the sequence affected the memorization of that number. As shown in figure 1. C, the average accuracy of target number in all eight positions was above eighty percent, and no significant difference was found among positions ($p>0.05$, one-way ANOVA). Then, the accuracy of the first half and second half of all blocks in each session were compared, and no significant difference between two halves was found ($P>0.05$, paired t-test, Figure 1. D). This indicated that during each session, the performance of participants remained stable. Fourteen out of eighteen participants conducted the task twice, with recording captured in either left- or right-sided brain regions. We tested the accuracy between two sessions for these fourteen participants. As shown in figure 1. E, most participants made more mistakes in the second session. But four of them performed much better in the second session. The bad performance of these four participants in the first session may be caused by maladaptive to the environment. After removal of these four participants, accuracy of remaining participants was significantly lower during the second session as compared to the first session (paired t test: $t9 = 2.5866$, $p<0.05$; Fig. 1F).

Attention modulates neural activity

Studies based on fMRI functional connectivity analysis, encephalographic (EEG) event-related potential (ERP) and repetitive TMS (rTMS) have identified dorsal lateral prefrontal cortex may serve as source of top-down modulation underlying visual attention (***Zanto et al.*** (***2010***); ***Zhang and Luck*** (***2008***); ***Zanto et al.*** (***2011***)). Human EEG and MEG studies showed increases in theta (3-7 Hz) activity in dorsal and ventral frontal regions, and anterior cingulate cortex (ACC) linked to attentional amplification (***McDermott et al.*** (***2017***); ***Szczepanski et al.*** (***2014***)). To test this, we analyzed the local field potential (LFP) recorded in dpPFC, dlPFC, mPFC, and STN while patients performed a novel non-motor decision-making task (Fig. 2A). The average power was computed separately across all attended and ignored trials during each session. In line with previous studies, theta power in dlPFC showed significantly increases during the attended trials than ignored trials (Fig. 2B). Other regions exhibited tendency to initially increase then decrease in theta power under both conditions, but the differences between conditions were not significant (Fig. 2B). Cross all sessions, beta power in dpPFC and dlPFC exhibited decreases following the presentation of stimulus under both conditions (Fig. 2C). The beta power in STN remain stable during the attended trials, and first increased then decreased during the ignored trials (Fig. 2C).

Some researchers investigate the effect of attention on inter-trial phase coherence at pre-stimulus low-frequency oscillations in area MT of monkey. Their results reveal that phase coherence in theta band increases when attention is deployed towards the receptive field of the recorded neuron (***Zareian et al.*** (***2020***)). In our study, we compared intertrial phase coherence (ITPC) between the attended and ignored conditions in frontal regions and STN (Fig. 3A). The ITPC under ignored condition (Fig. 3A, left panel) was significantly higher than the attended condition (Fig. 3A, right panel), which was different from study in area MT of monkey (Fig. 3A, middle panel). Cluster-based statistics confirmed statistically significant clusters, comprising delta, theta, alpha, and beta band in three prefrontal regions, and theta, alpha, and beta band in STN (Fig. 3A, right panel). The clusters in three prefrontal regions were last the whole trial duration, and the clusters in STN were spread in the late part of trial duration.

Attention modulates neural activity

We next examined the coherence between areas. We found the coherence in ignored trials was higher than in attended trials among all area pairs (Fig. 4A, left and middle panels). The coherence between dpPFC and STN was significantly different in delta, theta, alpha, and beta bands cross the whole trial duration (cluster-based permutation test). The coherence between dlPFC and STN were significantly different in theta, alpha, and beta band, beginning at 100ms after stimulus presentation and last several hundred milliseconds after stimulus disappear (cluster-based permutation test). The coherence between mPFC and STN was significantly different in theta, alpha, and beta bands, during the whole trial. The coherence between prefrontal regions was significantly different in alpha and beta bands, cross the whole trial duration (cluster-based permutation test).

In order to uncover the direction of functional interactions between each area pair, we adopted Granger causality analysis. We found significant STN leading information flow to dpPFC in theta band ($p<0.05$, paired t-test), to dlPFC in theta and alpha band ($P<0.05$, paired t-test), and to mPFC in high theta, alpha and beta band ($P<0.05$, paired t-test), in all trials. The information flow from dpPFC to STN in high beta band ($p<0.05$, paired t-test), from mPFC to STN in delta band ($p<0.05$, paired t-test). We observed significant information from dlPFC to dpPFC in alpha band, from mPFC to dpPFC in delta and theta band, and from dlPFC to mPFC in alpha band.

Our results show that the communication between brain areas was achieved through different oscillation bands. The theta band played an important role in communication between frontal regions and STN.

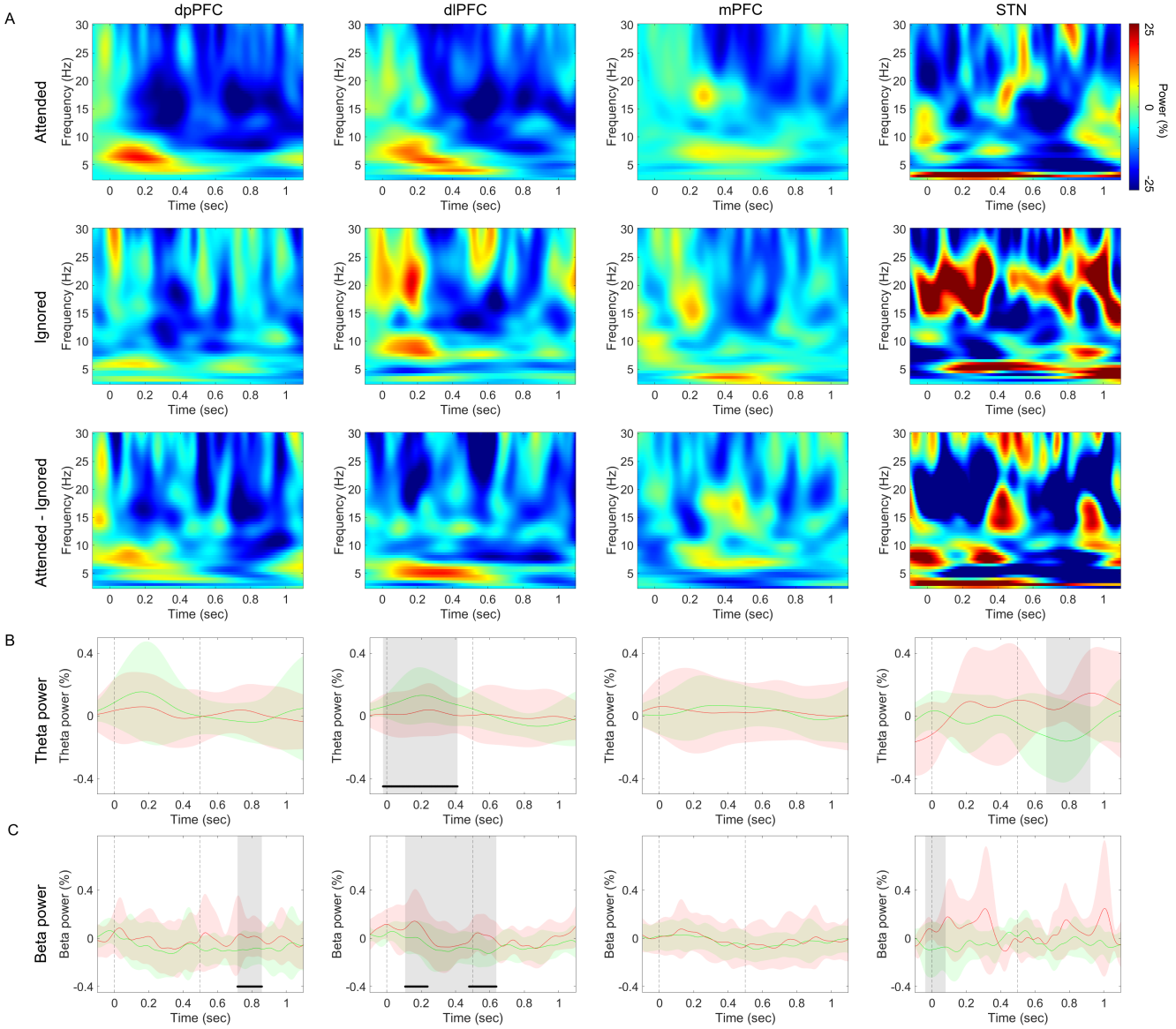

Figure 2. (A) Normalized oscillatory power averaged across all dpPFC electrodes (left), all dlPFC electrodes (left-middle), all mPFC electrodes (middle-right), and all STN electrodes (right). In each brain region, the power was averaged across attended trials (top), ignored trials (middle), and attended minus ignored (bottom). Stimulus onset time is denoted by time point zero on the X-axis. (B) Normalized oscillatory power averaged across electrodes located in each brain region, across theta band. Time points exhibiting a significant difference between each condition ($p < 0.05$, cluster-based permutation test) are denoted by black horizontal bar. Time points exhibiting a tendency to show difference between each condition ($p < 0.1$, cluster-based permutation test) are denoted by gray shaded box. Stimulus onset time is denoted by time point zero on the X-axis. (C) Same as (B), but averaged across the theta band.

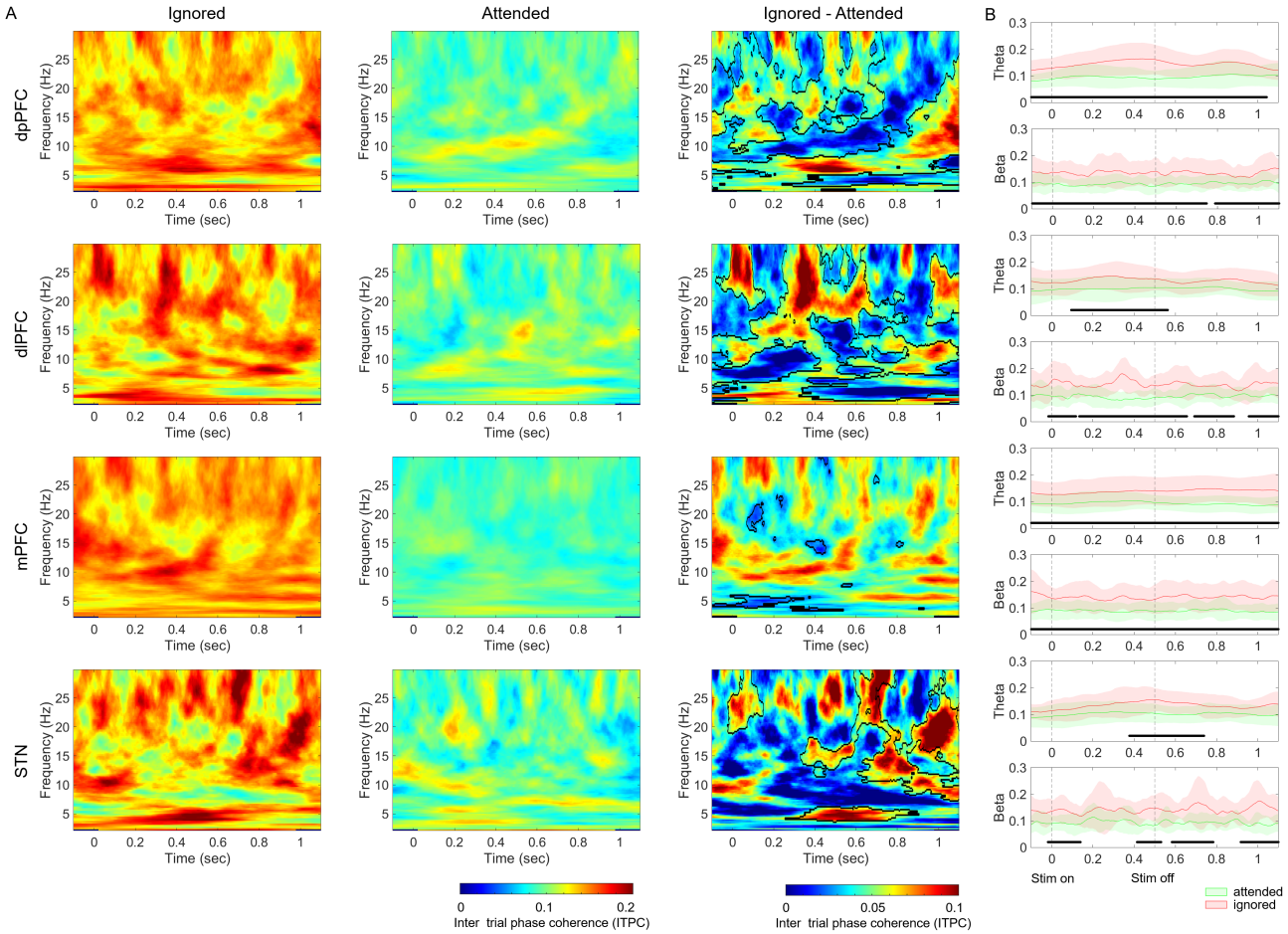

Figure 3. (A) Inter trial phase coherence (ITPC) averaged across all dpPFC electrodes (top), all dlPFC electrodes (top-middle), all mPFC electrodes (middle-bottom), all STN electrodes (bottom). In each brain region, the ITPC was averaged across ignored trials (left), attended trials (middle), and ignored minus attended (right). Mask in the right panel denotes time-frequency regions exhibiting significant differences between conditions ($p < 0.05$, cluster-based permutation test). Stimulus onset time is denoted by time point zero on the X-axis. (B) Same as (A), but averaged across the beta and theta band. Time points exhibiting a significant difference between each condition ($p < 0.05$, cluster-based permutation test) are denoted by black horizontal bar.

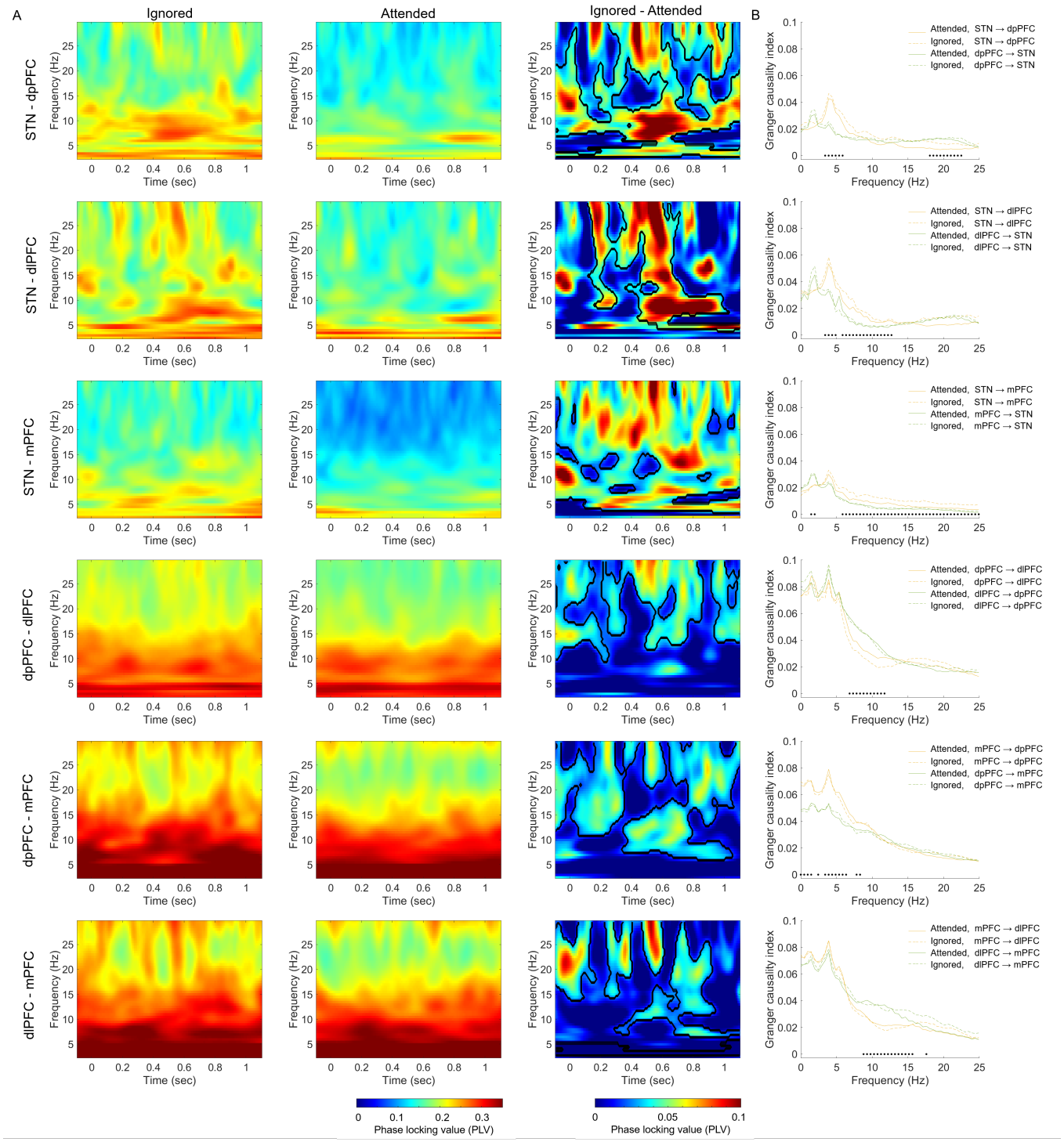

Figure 4. (A) Phase locking value (PLV) averaged across all STN-mPFC electrode pairs (top), all dpPFC-dlPFC electrode pairs (top-middle), all dpPFC-mPFC electrode pairs (middle-bottom), all dlPFC-mPFC electrodes (bottom). In each brain region, the PLV was averaged across ignored trials (left), attended trials (middle), and ignored minus attended (right). Mask in the right panel denotes time-frequency regions exhibiting significant differences between conditions ($p < 0.05$, cluster-based permutation test). Stimulus onset time is denoted by time point zero on the X-axis. (B) Granger causality index across all STN-mPFC electrode pairs (top), all dpPFC-dlPFC electrode pairs (top-middle), all dpPFC-mPFC electrode pairs (middle-bottom), all dlPFC-mPFC electrodes (bottom). Black horizontal dots denote the frequencies that show significant differences between two opposite information transfer directions ($p < 0.05$, paired t-test).

Attention modulation is associated with theta-BHG coupling

As previous studies in nonhuman primates showed selective attention decreases the coupling between the amplitude of gamma oscillations and the phase of theta oscillations (***Spyropoulos et al.*** (***2018***); ***Esghaei et al.*** (***2015***)). We assessed whether any similar relationship existed among the different frequency bands (delta, theta, alpha, beta, high gamma) during attentional modulation processes in human prefrontal regions and STN. We examined PAC between a wide range of frequencies for phase data (2-30 Hz), and BHG for amplitude data (80-200 Hz) in all of the electrodes spread across four regions (Fig. 5A). We found significant coupling between the phase of the delta/theta signal (2-8 Hz) and BHG amplitude (80-200 Hz) during ignored trials compared to attended trials (Fig. 5B, C). We also observed alpha phase-BHG amplitude coupling in electrodes over dpPFC (Fig. 5A, right panel, top).

As PAC also serves as an important mechanism for inter-regional information transfer. We computed the cross-regional PAC in both phase-amplitude combinations between all four regions, for both attended trials and ignored trials (Fig. 6A; Supplement figures 1-5, A). The inter-regional PAC was quantified as the coupling between the low-frequency phases (2-30 Hz) from the electrode in one region and the high-frequency amplitude (80-200 Hz) from the electrode in another region. The results showed that the delta/theta-BHG coupling were different between attended trials and ignored trials for all region pairs (Fig. 6A; Supplement figures 1-5, A). To further compare the coupling strength between different trials in all regional combinations, the mean of cross-regional PAC of the delta/theta-BHG bands was extracted. With post hoc paired t-test evaluation, we found that the coupling strength during the ignored trials was significantly greater than during the attended trials (Fig. 6B, C; Supplement figures 1-5, B, C).

Discussion

STN participated in attention modulation

Electrophysiological studies have shown that low-frequency interactions between PFC and STN support cognitive control, where fronto-STN circuits pause behavior and cognition when stop signals or conflict signals occur (***Frank et al.*** (***2007***); ***Aron et al.*** (***2016***); ***Zeng et al.*** (***2021***)). Theta activity of the PFC was shown to drive the activity of the STN, which adjusted the threshold of evidence in a dot motion discrimination task (***Zavala et al.*** (***2014***)). The STN DBS disrupted the correlation between PFC theta power and behavior responses (***Cavanagh et al.*** (***2011***)). The information flow seemed to be bidirectional, as a human intracranial study showed that STN stimulation evoked short-latency lateral PFC and motor cortical responses (12 ms) by using electrical stimulation tract-tracing (ESTT) (***Kelley et al.*** (***2017***)). The same study also revealed 4-Hz Granger causal connectivity from STN to midfrontal EEG during conflict tasks, and 4-Hz STN DBS improved cognitive performance (***Kelley et al.*** (***2017***)).

In our study, we found STN participated in attention modulation and fronto-STN circuits support this modulation process. ITPC in the STN during attended trials is significantly lower than ignored trials across theta, alpha, and beta bands, in line with a previous brain-computer interface (BCI) paradigms in EEG (***Zareian et al.*** (***2020***)). The theta-BHG coupling during attended trials is significantly lower than ignored trials and the BHG activities in prefrontal regions were coupled to theta phase in STN during ignored trials. The coherence between STN and frontal regions was significantly higher during the ignored trials than attended trials. The GC analysis showed that theta activity in STN casually drove the theta activity in prefrontal regions during the task.

Within and cross-region phase-amplitude coupling support attention modulation

Researchers used LFP power recorded from area MT of macaque to decode the context the animal was attending to. Both delta/theta (<9 Hz) and broadband gamma (31-120 Hz) activities contain sufficient information to decode (***Esghaei and Daliri*** (***2014***)). By examining LFP data from large-scale ECoG recordings, researchers revealed that attentional allocation and behavioral performance fluc-

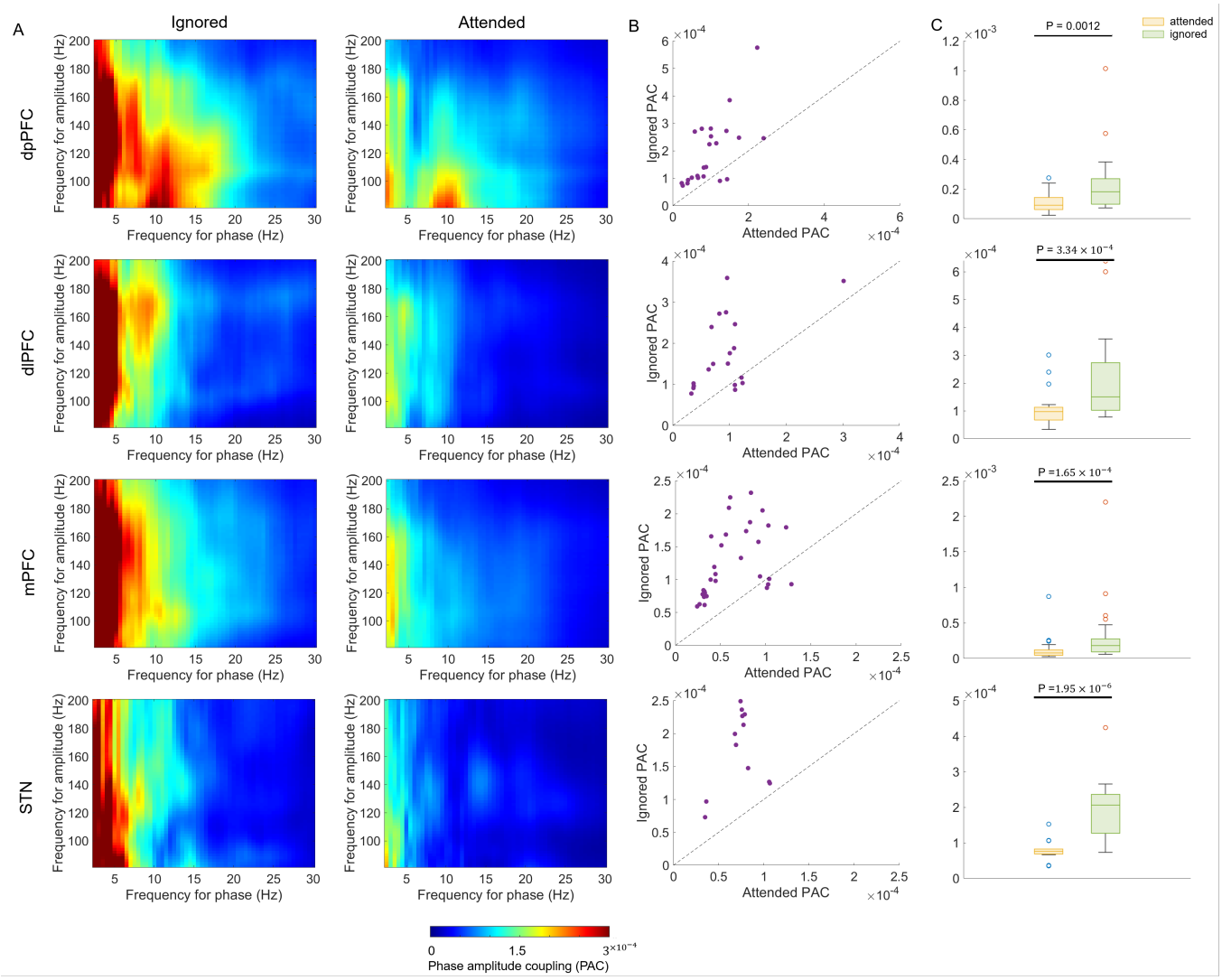

Figure 5. (A) Phase amplitude coupling (PAC) averaged across all dpPFC electrodes (top), all dlPFC electrodes (top-middle), all mPFC electrode pairs (middle-bottom), all STN electrodes (bottom). In each brain region, the PAC was averaged across ignored trials (left) and attended trials (right). (B) Individual electrode's PAC values for attended and ignored trials. Each circle represents data from a single electrode with PAC calculated separately for attended trials (X-axis) and ignored trials (Y-axis). (C) Bar plot showing group average of PAC values over theta phase frequencies (4-8 Hz) and BHG amplitude frequencies (80-200 Hz) for attended and ignored trials, across electrodes in each brain region. Error bars represent standard deviation.

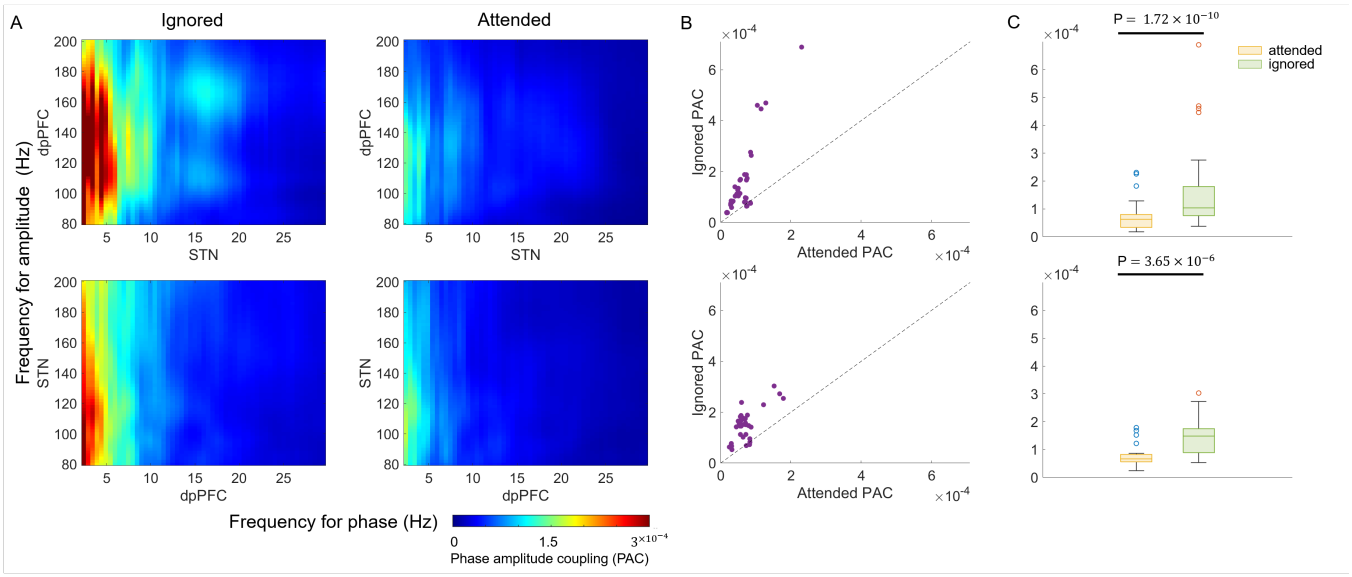

Figure 6. (A) Phase amplitude coupling (PAC) for low-frequency phase from dpPFC and BHG frequency amplitude from STN averaged across all electrode pairs (top), for low-frequency phase from STN and BHG frequency amplitude from dpPFC averaged across all electrode pairs (bottom). For each coupling pair, the PAC was averaged across ignored trials (left) and attended trials (right). (B) Individual electrode pair's PAC values for attended and ignored trials. Each circle represents data from a single electrode pair with PAC calculated separately for attended trials (X-axis) and ignored trials (Y-axis). (C) Bar plot showing group average of PAC values over theta phase frequencies (4-8 Hz) and BHG amplitude frequencies (80-200 Hz) for attended and ignored trials, across electrode pairs across brain regions. Error bars represent standard deviation.

Figure 6—figure supplement 1. Phase amplitude coupling (PAC) between dlPFC and STN

Figure 6—figure supplement 2. Phase amplitude coupling (PAC) between dpPFC and dlPFC

Figure 6—figure supplement 3. Phase amplitude coupling (PAC) between mPFC and STN

Figure 6—figure supplement 4. Phase amplitude coupling (PAC) between dlPFC and mPFC

Figure 6—figure supplement 5. Phase amplitude coupling (PAC) between dpPFC and mPFC

tuate as a function of the theta phase in widespread regions of the frontoparietal attention network. They hypothesized that low-frequency oscillations are a direct result of periodic fluctuations and cortical high-frequency band (HFB) is modulated by the low-frequency activity (***Helfrich et al.*** (***2018***)). In our study, the theta-BHG coupling in frontal regions and STN was modulated between attended trials and ignored trials. The theta-BHG PAC was significantly higher during the ignored trials than the attended trials. As BHG activities are sufficient proxy for local spiking activities, our results were in line with previous study performed on macaque monkey, in which attentional desynchronization was mediated by de-coupling between local spiking activities and low-frequency oscillations (***Fries et al.*** (***2001***); ***Buffalo et al.*** (***2011***); ***Esghaei et al.*** (***2018***)).

Our cross-region PAC analysis also showed that the coupling between theta phase from one region and high gamma amplitude from another region was significantly higher during the ignored trials than attended trials. As low-frequency coherence between regions was significantly higher during ignored trials, we believe the cross-regional PAC coupling was mediated by the coherent cross-regional low-frequency. GC analysis showed significant theta band connectivity from STN to frontal regions, we believed that theta activity in STN drove the activity in frontal regions during cognitive tasks.

Limitations and future work

Our study was performed on frontal regions and STN. All of these areas are related to higher-order cognitive modulation. As attention is a meta modulation process between sensory areas and high-order cognitive control areas (***Buffalo et al.*** (***2011***); ***Fries et al.*** (***2008***); ***Chalk et al.*** (***2010***); ***Mitchell et al.*** (***2009***); ***Cohen and Maunsell*** (***2009***); ***Averbeck et al.*** (***2006***)), further research on the relationship between sensory areas, frontal regions and STN need to be done.

We used GC analysis to identify the relationship between STN and frontal regions. As GC is a statistical test for determining whether one time series can predict another, it does not provide any insight into the true causality (***Shojaie and Fox*** (***2022***)). Future studies using direct brain stimulation can reveal more solid causal effects between areas.

Conclusion

In this study, we re-analyzed neural data recorded in Parkinson's patients during attended and ignored states. The results suggested that STN participated in attention processing. STN theta activity drove the activity in frontal regions during the cognitive task. PAC between theta band and BHG within and cross regions located in prefrontal areas and STN was basic mechanism for attention modulation.

Methods and Materials

The dataset we used was from research (***Zavala et al.*** (***2017***)). The information of participants, task, iEEG recordings, and electrode localization was reported in detail in (***Zavala et al.*** (***2017***)). Here, we introduce them in brief.

Participants

18 patients undergoing deep brain stimulation (DBS) surgery for Parkinson's disease participated. This study used data from all participants for behavioral analysis, and data from 9 participants for local field potential analysis, in order to get relatively balanced attended and ignored trials.

Behavioral task

Participants performed a novel working memory task with non-motor decision-making during the task. Each task session involved 30 blocks. At the beginning of each block, an image of square or octagon was displayed on the screen to indicate the target shape for the upcoming block. During each block, participants were sequentially presented with eight randomly chosen single-digit numbers within a square or an octagon, and instructed to attend to and remember the numbers within

the target shape. Each number was displayed for 500 ms, following a blank screen for 500 ± 100 ms. During the presentation of the numbers, participants were instructed to limit all movements if possible. At the end of each block, the participants were prompted to vocally retrieve the four target numbers. Fourteen participants performed one session while LFP recordings were captured from the left STN and a second session while LFP recordings were captured from the right STN.

Time frequency analysis

We performed all analyses using custom MATLAB scripts based on fieldtrip toolbox (***Oostenveld et al.*** (***2011***)). The original local field potential (LFP) activity from each macroelectrode and iEEG activity from each subdural contact were bandpass filtered between 1 and 500 Hz, downsampled to 1 kHz, and notch filtered at 60 Hz. Trials that number was presented in the target shape and successfully retrieved were defined as "attended" trials. Trials that number was presented in the target shape but not retrieved at the end of block were defined as "ignored" trials. We calculated accuracy of each session as the ratio of target trials that were successfully retrieved to all target trials. In order to get relatively balanced trials under both conditions, sessions with accuracy larger than 80% were discarded. Time frequency measures were computed as multiplication between the power spectrum of LFP signals and the power spectrum of complex Morlet wavelets, with frequency increasing from 2 to 200 Hz. We used a 1000 ms buffer on both sides of the clipped data to eliminate edge effects. We chose 500 ms preceding the presentation of each number as baseline period and calculated the percentage change in power (normalized power) by comparing the power to the mean power recorded during the baseline period. For each brain region, we average the normalized power from all electrodes within that brain region. The above procedures were repeated across trials separately for "attended" and "ignored" trials.

Inter trial phase coherence

Inter trial phase coherence (ITPC) is a measure of how consistent the oscillatory phase is across trials. Here, we used the Fourier spectrum achieved through the wavelet analysis to investigate phase relationships of low frequency (2-30 Hz) for each electrode across attended trials and ignored trials. ITPC was indexed according to the following formula (***Diepen and Mazaheri*** (***2018***)):

$$ITPC(f,t) = \frac{1}{N}\left|\sum_{k=1}^{N} e^{i\phi^k(f,t)}\right|$$

Where N is the number of trials, ϕ^k is the instantaneous phase of the signal at frequency f and time t in trial k.

Inter-regional coherence

To quantify the time-varying coherence between two brain regions, we calculated the phase locking value (PLV) between every pair of electrodes from two brain regions at each time-frequency point. The PLV was indexed according to the following formula (***Lachaux et al.*** (***1999***)):

$$PLV_{(f,t)} = \frac{1}{N}\left|\sum_{k=1}^{N} e^{i\phi^k(f,t)}\right|$$

Where, $\theta^k(f,t)$ is the phase difference for electrode pair (a, b), at frequency f and time t in trial k. N is the number of trials. PLV ranger from 0 to 1, with higher value if the phase differences between electrodes vary less across time.

Granger causality

To examine the directionality of the information flow between two brain regions, we analyzed the cross-regional connectivity with spectral Granger causality. Spectral Granger causality quantifies the directional connectivity strength by testing the prediction error of the signal by introducing

time series from another brain region in the frequency domain. We extracted the GC values within the low-frequency band (2-30 Hz) for electrode pairs each from one brain region across attended and ignored trials, separately. The significance testing for the spectral GC was conducted by cluster-based non-parametric permutation methods (***Maris and Oostenveld*** (***2007***)).

Phase amplitude coupling

To identify the cross-frequency coupling in each brain region, we examined modulation index (MI) between low frequencies (2-30 Hz) for phase data and BHG (80-200 Hz) for amplitude data in each electrode localized in each brain region. The calculation followed the procedure outlined by Tort and colleagues (***Tort et al.*** (***2010***)).

Phase amplitude coupling

During behavior analysis, we performed one-way ANOVA with post-hoc Tukey's multiple comparison test for the accuracy comparison of target numbers presented in different positions. The accuracy between two sessions, two parts in one session, and PAC between theta-broadband high gamma was evaluated by two-sided paired t-test.

The comparison of theta/beta band LFP power, ITPC, time-frequency cross-regional coherence, and GC between attended and ignored trials were evaluated by cluster-based non-parametric permutation procedure (number of permutations was 10000, threshold of significance if 0.05) (***Maris and Oostenveld*** (***2007***)).

Acknowledgments

We thank Sen Wan and Yanwang Zhai for very fruitful discussions.

Data availability

The original data can be found in this excellent paper (***Zavala et al.*** (***2017***)).

Funding

This work was supported by the Science Center of National Natural Science Foundation of China "Cognitive Computing" (No. 62088102), Major Project of New Generation artificial intelligence of Ministry of Science and Technology, (No. 2020AAA0105500).

Author contributions

Q. D. and J. W. conceived and designed the project. S. A. analyzed the data. S. A., J. W., and Q. D. prepared figures and wrote the manuscript with input from all authors.

References

Aron A, Herz D, Brown P, Forstmann B, Zaghloul K. Frontosubthalamic Circuits for Control of Action and Cognition. Journal of Neuroscience. 2016 11; 36:11489–11495. doi: 10.1523/JNEUROSCI.2348-16.2016.

Averbeck B, Latham P, Pouget A. Neural correlations, population coding and computation. Nature reviews Neuroscience. 2006 06; 7:358–66. doi: 10.1038/nrn1888.

Baird B, Smallwood J, Lutz A, Schooler JW. The Decoupled Mind: Mind-wandering Disrupts Cortical Phase-locking to Perceptual Events. Journal of Cognitive Neuroscience. 2014 11; 26(11):2596–2607. https://doi.org/10.1162/jocn_a_00656, doi: 10.1162/jocn_a_00656.

Buckley, Mark, J, Mansouri, Farshad, A, Hoda, Hassan, Mahboubi, and M. Dissociable Components of Rule-Guided Behavior Depend on Distinct Medial and Prefrontal Regions. Science. 2009; .

Buffalo E, Fries P, Landman R, Buschman T, Desimone R. Laminar differences in gamma and alpha coherence in the ventral stream. Proceedings of the National Academy of Sciences of the United States of America. 2011 06; 108:11262–7. doi: 10.1073/pnas.1011284108.

Buschman T, Kastner S. From Behavior to Neural Dynamics: An Integrated Theory of Attention. Neuron. 2015; 88(1):127–144. https://www.sciencedirect.com/science/article/pii/S0896627315007746, doi: https://doi.org/10.1016/j.neuron.2015.09.017.

Cavanagh J, Wiecki T, Cohen M, Figueroa C, Samanta J, Sherman S, Frank M. Subthalamic nucleus stimulation reverses mediofrontal influence over decision threshold. Nature neuroscience. 2011 09; 14:1462–7. doi: 10.1038/nn.2925.

Chalk M, Herrero J, Gieselmann M, Delicato L, Gotthardt S, Thiele A. Attention Reduces Stimulus-Driven Gamma Frequency Oscillations and Spike Field Coherence in V1. Neuron. 2010 04; 66:114–25. doi: 10.1016/j.neuron.2010.03.013.

Cohen M, Maunsell J. Attention improves performance primarily by reducing interneuronal correlations. Nature neuroscience. 2009 11; 12:1594–600. doi: 10.1038/nn.2439.

Corbetta M, Shulman GL. Control of goal-directed and stimulus-driven attention in the brain. Nature Reviews Neuroscience. 2002; 3(3):201.

Coxon J, Impe A, Wenderoth N, Swinnen S. Aging and Inhibitory Control of Action: Cortico-Subthalamic Connection Strength Predicts Stopping Performance. The Journal of neuroscience : the official journal of the Society for Neuroscience. 2012 06; 32:8401–12. doi: 10.1523/JNEUROSCI.6360-11.2012.

Diepen R, Mazaheri A. The Caveats of observing Inter-Trial Phase-Coherence in Cognitive Neuroscience. Scientific Reports. 2018 02; 8. doi: 10.1038/s41598-018-20423-z.

Drummond N, Chen R. Deep Brain Stimulation and Recordings: Insights into the contributions of subthalamic nucleus in cognition. NeuroImage. 2020 08; 222:117300. doi: 10.1016/j.neuroimage.2020.117300.

Dubey A, Markowitz DA, Pesaran B. Top-down control of exogenous attentional selection is mediated by beta coherence in prefrontal cortex. Neuron. 2023; 111(20):3321–3334.e5. https://www.sciencedirect.com/science/article/pii/S0896627323005068, doi: https://doi.org/10.1016/j.neuron.2023.06.025.

Eliasmith C, Stewart T, Choo X, Bekolay T, Dewolf T, Tang C, Rasmussen D. A Large-Scale Model of the Functioning Brain. Science (New York, NY). 2012 11; 338:1202–5. doi: 10.1126/science.1225266.

Esghaei M, Daliri M. Decoding of Visual Attention from LFP Signals of Macaque MT. PloS one. 2014 06; 9:e100381. doi: 10.1371/journal.pone.0100381.

Esghaei M, Daliri mr, Treue S. Attention Decreases Phase-Amplitude Coupling, Enhancing Stimulus Discriminability in Cortical Area MT. Frontiers in Neural Circuits. 2015 12; 9. doi: 10.3389/fncir.2015.00082.

Esghaei M, Daliri mr, Treue S. Attention decouples action potentials from the phase of local field potentials in macaque visual cortical area MT. BMC Biology. 2018 08; 16. doi: 10.1186/s12915-018-0551-2.

Forstmann B, Keuken M, Jahfari S, Bazin PL, Neumann J, Schäfer A, Anwander A, Turner R. Cortico-subthalamic white matter tract strength predict interindividual efficacy in stopping a motor response. NeuroImage. 2012 03; 60:370–5. doi: 10.1016/j.neuroimage.2011.12.044.

Foster BL, Kaveh A, Dastjerdi M, Miller KJ, Parvizi J. Human Retrosplenial Cortex Displays Transient Theta Phase Locking with Medial Temporal Cortex Prior to Activation during Autobiographical Memory Retrieval. Journal of Neuroscience. 2013; 33(25):10439–10446. https://www.jneurosci.org/content/33/25/10439, doi: 10.1523/JNEUROSCI.0513-13.2013.

Foxe JJ, Snyder AC. The Role of Alpha-Band Brain Oscillations as a Sensory Suppression Mechanism during Selective Attention. Frontiers in Psychology. 2011; 2.

Frank M, Samanta J, Moustafa A, Sherman S. Hold Your Horses: Impulsivity, Deep Brain Stimulation, and Medication in Parkinsonism. Science (New York, NY). 2007 12; 318:1309–12. doi: 10.1126/science.1146157.

Fries P, Reynolds JH, Rorie AE, Desimone R. Modulation of Oscillatory Neuronal Synchronization by Selective Visual Attention. Science. 2001; 291(5508):1560–1563. https://www.science.org/doi/abs/10.1126/science.1055465, doi: 10.1126/science.1055465.

Fries P, Womelsdorf T, Oostenveld R, Desimone R. The Effects of Visual Stimulation and Selective Visual Attention on Rhythmic Neuronal Synchronization in Macaque Area V4. The Journal of neuroscience : the official journal of the Society for Neuroscience. 2008 05; 28:4823–35. doi: 10.1523/JNEUROSCI.4499-07.2008.

Gregoriou GG, Rossi AF, Ungerleider LG, Desimone R. Lesions of prefrontal cortex reduce attentional modulation of neuronal responses and synchrony in V4. Nature Neuroscience. 2014; 17(7):1003–1011.

Haciahmet C, Frings C, Pastötter B. Target amplification and distractor inhibition: Theta oscillatory dynamics of selective attention in a flanker task. Cognitive Affective & Behavioral Neuroscience. 2021 03; doi: 10.3758/s13415-021-00876-y.

Haynes W, Haber S. The Organization of Prefrontal-Subthalamic Inputs in Primates Provides an Anatomical Substrate for Both Functional Specificity and Integration: Implications for Basal Ganglia Models and Deep Brain Stimulation. The Journal of neuroscience : the official journal of the Society for Neuroscience. 2013 03; 33:4804–14. doi: 10.1523/JNEUROSCI.4674-12.2013.

Helfrich R, Fiebelkorn I, Szczepanski S, Lin J, Parvizi J, Knight R, Kastner S. Neural Mechanisms of Sustained Attention Are Rhythmic. Neuron. 2018 08; 99:854–865.e5. doi: 10.1016/j.neuron.2018.07.032.

Helfrich R, Knight R. Oscillatory Dynamics of Prefrontal Cognitive Control. Trends in Cognitive Sciences. 2016 10; 20. doi: 10.1016/j.tics.2016.09.007.

Herz DM, Tan H, Brittain JS, Fischer P, Cheeran B, Green AL, FitzGerald J, Aziz TZ, Ashkan K, Little S, Foltynie T, Limousin P, Zrinzo L, Bogacz R, Brown P. Distinct mechanisms mediate speed-accuracy adjustments in cortico-subthalamic networks. eLife. 2017 jan; 6:e21481. https://doi.org/10.7554/eLife.21481, doi: 10.7554/eLife.21481.

Kelley R, Flouty O, Emmons E, Kim Y, Kingyon J, Wessel J, Oya H, Greenlee J, Narayanan N. A human prefrontal-subthalamic circuit for cognitive control. Brain : a journal of neurology. 2017 11; 141. doi: 10.1093/brain/awx300.

King A, Linke J, Gass A, Hennerici M, Tost H, Poupon C, Wessa M. Microstructure of a three-way anatomical network predicts individual differences in response inhibition: A tractography study. NeuroImage. 2011 09; 59:1949–59. doi: 10.1016/j.neuroimage.2011.09.008.

Kühn A, Hariz M, Silberstein P, Tisch S, Kupsch A, Schneider GH, Limousin-Dowsey P, Yarrow K, Brown P. Activation of the subthalamic region during emotional processing in Parkinson disease. Neurology. 2005 10; 65:707–13. doi: 10.1212/01.wnl.0000174438.78399.bc.

Lachaux JP, Rodriguez E, Martinerie J, Varela FJJ. Measuring Phase Synchrony in Brain Signals. Human brain mapping. 1999 01; 8:194–208. doi: 10.1002/(SICI)1097-0193(1999)8:43.0.CO;2-C.

Maris E, Oostenveld R. Nonparametric statistical testing of EEG- and MEG-data. Journal of neuroscience methods. 2007 09; 164:177–90. doi: 10.1016/j.jneumeth.2007.03.024.

McDermott T, Wiesman A, Proskovec A, Heinrichs-Graham E, Wilson T. Spatiotemporal Oscillatory Dynamics of Visual Selective Attention during a Flanker Task. NeuroImage. 2017 05; 156. doi: 10.1016/j.neuroimage.2017.05.014.

Mitchell J, Sundberg K, Reynolds J. Spatial Attention Decorrelates Intrinsic Activity Fluctuations in Macaque Area V4. Neuron. 2009 09; 63:879–88. doi: 10.1016/j.neuron.2009.09.013.

Moore T, Zirnsak M. Neural Mechanisms of Selective Visual Attention. Annual Review of Psychology. 2017; 68(1):47–72. https://doi.org/10.1146/annurev-psych-122414-033400, doi: 10.1146/annurev-psych-122414-033400, pMID: 28051934.

Nambu A, Tokuno H, Takada M. Functional significance of the cortico–subthalamo–pallidal 'hyperdirect' pathway. Neuroscience research. 2002 07; 43:111–7. doi: 10.1016/S0168-0102(02)00027-5.

Oostenveld R, Fries P, Maris E, Schoffelen JM. FieldTrip: Open Source Software for Advanced Analysis of MEG, EEG, and Invasive Electrophysiological Data. Computational intelligence and neuroscience. 2011 01; 2011:156869. doi: 10.1155/2011/156869.

Popov T, Steffen A, Weisz N, Miller G, Rockstroh B. Cross-frequency dynamics of neuromagnetic oscillatory activity: Two mechanisms of emotion regulation. Psychophysiology. 2013 02; 49. doi: 10.1111/j.1469-8986.2012.01484.x.

Ray S, Maunsell J. Different Origins of Gamma Rhythm and High-Gamma Activity in Macaque Visual Cortex. PLoS biology. 2011 04; 9:e1000610. doi: 10.1371/journal.pbio.1000610.

Seeley WW, Menon V, Schatzberg AF, Keller J, Glover GH, Kenna H, Reiss AL, Greicius MD. Dissociable Intrinsic Connectivity Networks for Salience Processing and Executive Control. Journal of Neuroscience. 2007; 27(9):2349–2356. https://www.jneurosci.org/content/27/9/2349, doi: 10.1523/JNEUROSCI.5587-06.2007.

Shojaie A, Fox E. Granger Causality: A Review and Recent Advances. Annual Review of Statistics and Its Application. 2022 03; 9. doi: 10.1146/annurev-statistics-040120-010930.

Spyropoulos G, Bosman C, Fries P. A theta rhythm in macaque visual cortex and its attentional modulation. Proceedings of the National Academy of Sciences. 2018 05; doi: 10.1101/117804.

Suzuki M, Gottlieb J. Distinct neural mechanisms of distractor suppression in the frontal and parietal lobe. Nature Neuroscience. 2013; 16(1):98–U139.

Szczepanski S, Crone N, Kuperman R, Auguste K, Parvizi J, Knight R. Dynamic Changes in Phase-Amplitude Coupling Facilitate Spatial Attention Control in Fronto-Parietal Cortex. PLoS biology. 2014 08; 12:e1001936. doi: 10.1371/journal.pbio.1001936.

Taylor P, Nobre A, Rushworth M. Subsecond Changes in Top–Down Control Exerted by Human Medial Frontal Cortex during Conflict and Action Selection: A Combined Transcranial Magnetic Stimulation–Electroencephalography Study. The Journal of neuroscience : the official journal of the Society for Neuroscience. 2007 11; 27:11343–53. doi: 10.1523/JNEUROSCI.2877-07.2007.

Tort A, Komorowski R, Eichenbaum H, Kopell N. Measuring Phase-Amplitude Coupling Between Neuronal Oscillations of Different Frequencies. Journal of neurophysiology. 2010 05; 104:1195–210. doi: 10.1152/jn.00106.2010.

Uddin L. Salience processing and insular cortical function and dysfunction. Nature Reviews Neuroscience. 2014 11; doi: 10.1038/nrn3857.

Vossel S, Weidner R, Driver J, Friston KJ, Fink GR. Deconstructing the architecture of dorsal and ventral attention systems with dynamic causal modeling. The Journal of Neuroscience : The Official Journal of the Society for Neuroscience. 2005; 32(31):10637–10648.

Watson B, Ding M, Buzsáki G. Temporal coupling of field potentials and action potentials in the neocortex. European Journal of Neuroscience. 2017 12; 48. doi: 10.1111/ejn.13807.

Wessel J, Diesburg D, Greenlee J. Non-selective inhibition of inappropriate motor-tendencies during response-conflict by a fronto-subthalamic mechanism. eLife Sciences. 2019 05; 8. doi: 10.7554/eLife.42959.

Zanto T, Rubens MT, Bollinger J, Gazzaley A. Top-down modulation of visual feature processing: The role of the inferior frontal junction. NeuroImage. 2010 11; 53:736–45. doi: 10.1016/j.neuroimage.2010.06.012.

Zanto T, Rubens MT, Thangavel A, Gazzaley A. Causal role of the prefrontal cortex in top-down modulation of visual processing and working memory. Nature neuroscience. 2011 03; 14:656–61. doi: 10.1038/nn.2773.

Zareian B, Maboudi K, Daliri mr, Moghaddam H, Treue S, Esghaei M. Attention strengthens across-trial prestimulus phase coherence in visual cortex, enhancing stimulus processing. Scientific Reports. 2020 03; 10. doi: 10.1038/s41598-020-61359-7.

Zavala B, Jang A, Trotta M, Lungu C, Brown P, Zaghloul K. Cognitive control involves theta power within trials and beta power across trials in the prefrontal-subthalamic network. Brain : a journal of neurology. 2018 10; 141. doi: 10.1093/brain/awy266.

Zavala B, Jang A, Zaghloul K. Human subthalamic nucleus activity during non-motor decision making. eLife. 2017 12; 6. doi: 10.7554/eLife.31007.

Zavala B, Tan H, Little S, Ashkan K, Hariz M, Foltynie T, Zrinzo L, Zaghloul K, Brown P. Midline Frontal Cortex Low-Frequency Activity Drives Subthalamic Nucleus Oscillations during Conflict. The Journal of neuroscience : the official journal of the Society for Neuroscience. 2014 05; 34:7322–33. doi: 10.1523/JNEUROSCI.1169-14.2014.

Zeng K, Drummond N, Ghahremani A, Saha U, Kalia S, Hodaie M, Lozano A, Aron A, Chen R. Fronto-subthalamic phase synchronization and cross-frequency coupling during conflict processing. NeuroImage. 2021 05; 238:118205. doi: 10.1016/j.neuroimage.2021.118205.

Zhang W, Luck S. Feature-based attention modulates feedforward visual processing. Nature neuroscience. 2008 12; 12:24–5. doi: 10.1038/nn.2223.

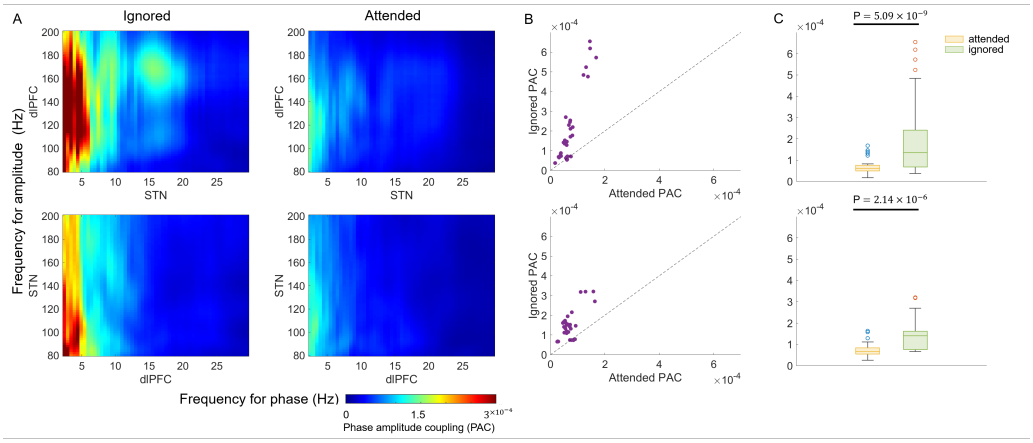

Figure 6—figure supplement 1. (A) Phase amplitude coupling (PAC) for low-frequency phase from dlPFC and BHG frequency amplitude from STN averaged across all electrode pairs (top), for low-frequency phase from STN and BHG frequency amplitude from dlPFC averaged across all electrode pairs (bottom). For each coupling pair, the PAC was averaged across ignored trials (left) and attended trials (right). (B) Individual electrode pair's PAC values for attended and ignored trials. Each circle represents data from a single electrode pair with PAC calculated separately for attended trials (X-axis) and ignored trials (Y-axis). (C) Bar plot showing group average of PAC values over theta phase frequencies (4-8 Hz) and BHG amplitude frequencies (80-200 Hz) for attended and ignored trials, across electrode pairs across brain regions. Error bars represent standard deviation.

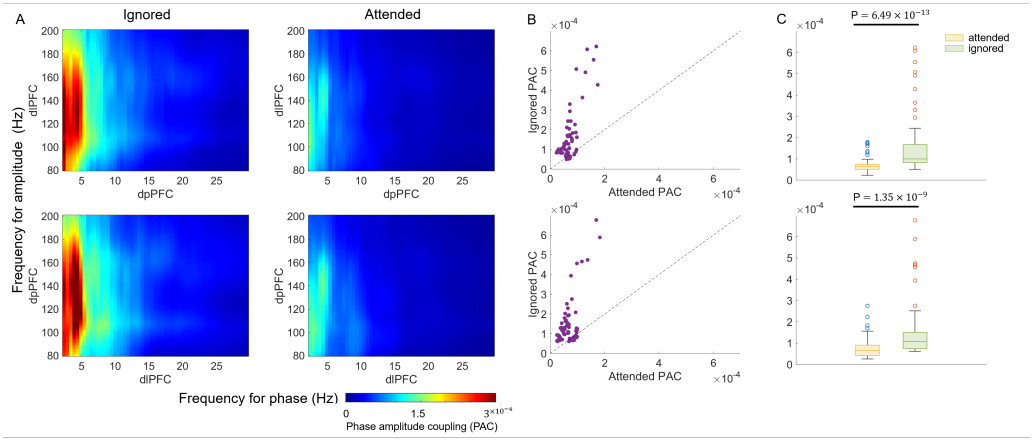

Figure 6—figure supplement 2. (A) Phase amplitude coupling (PAC) for low-frequency phase from dpPFC and BHG frequency amplitude from dlPFC averaged across all electrode pairs (top), for low-frequency phase from dlPFC and BHG frequency amplitude from dpPFC averaged across all electrode pairs (bottom). For each coupling pair, the PAC was averaged across ignored trials (left) and attended trials (right). (B) Individual electrode pair's PAC values for attended and ignored trials. Each circle represents data from a single electrode pair with PAC calculated separately for attended trials (X-axis) and ignored trials (Y-axis). (C) Bar plot showing group average of PAC values over theta phase frequencies (4-8 Hz) and BHG amplitude frequencies (80-200 Hz) for attended and ignored trials, across electrode pairs across brain regions. Error bars represent standard deviation.

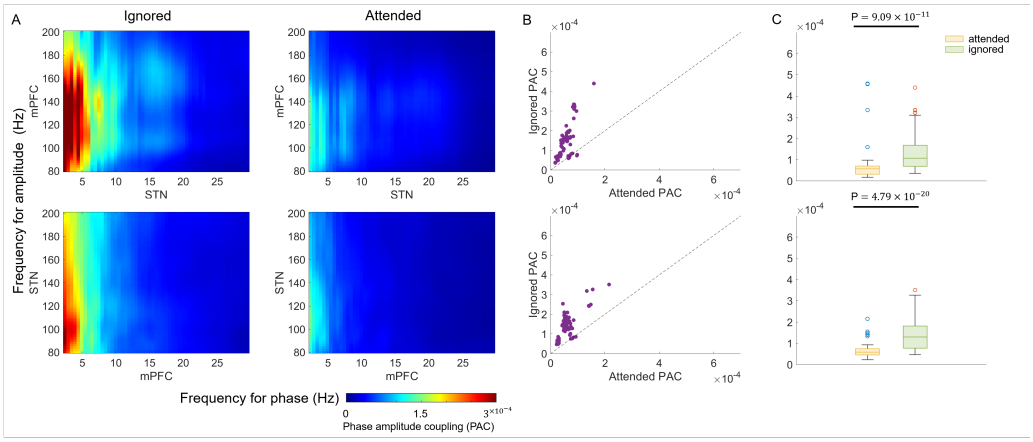

Figure 6—figure supplement 3. (A) Phase amplitude coupling (PAC) for low-frequency phase from STN and BHG frequency amplitude from mPFC averaged across all electrode pairs (top), for low-frequency phase from mPFC and BHG frequency amplitude from STN averaged across all electrode pairs (bottom). For each coupling pair, the PAC was averaged across ignored trials (left) and attended trials (right). (B) Individual electrode pair's PAC values for attended and ignored trials. Each circle represents data from a single electrode pair with PAC calculated separately for attended trials (X-axis) and ignored trials (Y-axis). (C) Bar plot showing group average of PAC values over theta phase frequencies (4-8 Hz) and BHG amplitude frequencies (80-200 Hz) for attended and ignored trials, across electrode pairs across brain regions. Error bars represent standard deviation.

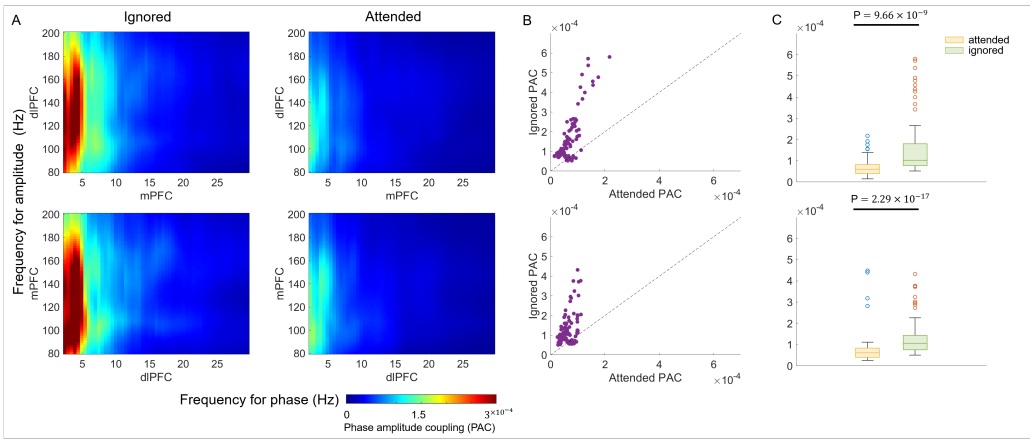

Figure 6—figure supplement 4. (A) Phase amplitude coupling (PAC) for low-frequency phase from dlPFC and BHG frequency amplitude from mPFC averaged across all electrode pairs (top), for low-frequency phase from mPFC and BHG frequency amplitude from dlPFC averaged across all electrode pairs (bottom). For each coupling pair, the PAC was averaged across ignored trials (left) and attended trials (right). (B) Individual electrode pair's PAC values for attended and ignored trials. Each circle represents data from a single electrode pair with PAC calculated separately for attended trials (X-axis) and ignored trials (Y-axis). (C) Bar plot showing group average of PAC values over theta phase frequencies (4-8 Hz) and BHG amplitude frequencies (80-200 Hz) for attended and ignored trials, across electrode pairs across brain regions. Error bars represent standard deviation.

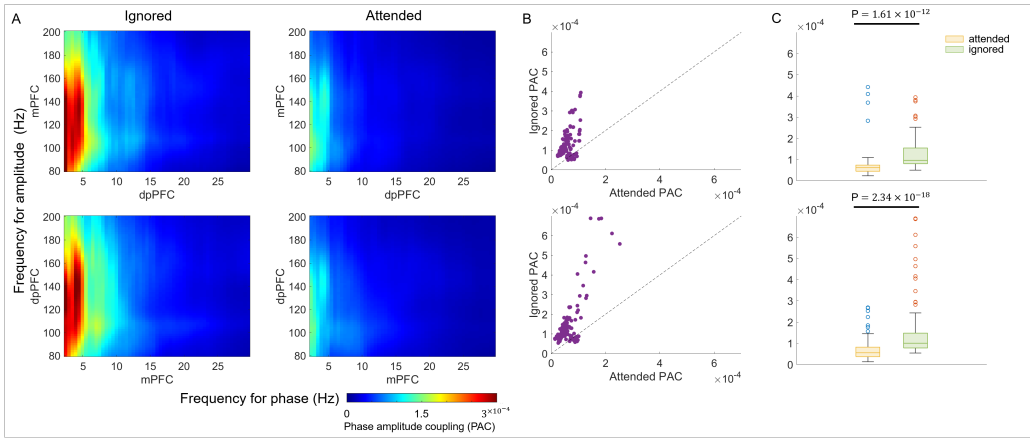

Figure 6—figure supplement 5. (A) Phase amplitude coupling (PAC) for low-frequency phase from dpPFC and BHG frequency amplitude from mPFC averaged across all electrode pairs (top), for low-frequency phase from mPFC and BHG frequency amplitude from dpPFC averaged across all electrode pairs (bottom). For each coupling pair, the PAC was averaged across ignored trials (left) and attended trials (right). (B) Individual electrode pair's PAC values for attended and ignored trials. Each circle represents data from a single electrode pair with PAC calculated separately for attended trials (X-axis) and ignored trials (Y-axis). (C) Bar plot showing group average of PAC values over theta phase frequencies (4-8 Hz) and BHG amplitude frequencies (80-200 Hz) for attended and ignored trials, across electrode pairs across brain regions. Error bars represent standard deviation.

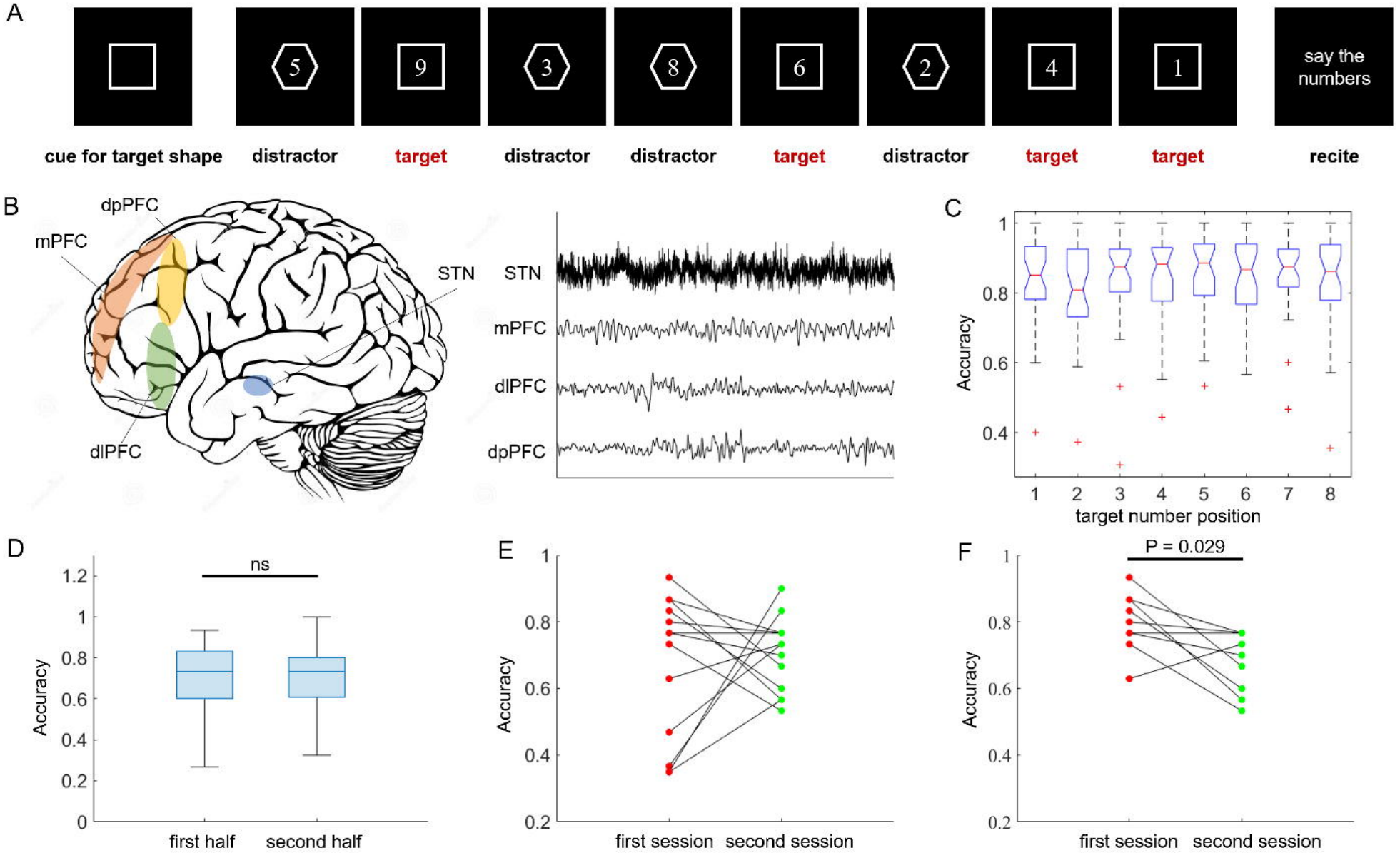
A
5
9
3
8
6
2
4
1
say the numbers
cue for target shape
distractor
target
distractor
distractor
target
distractor
target
target
recite
B
dpPFC
mPFC
STN
dlPFC
STN
mPFC
dlPFC
dpPFC
C
Accuracy
target number position
D
ns
Accuracy
first half
second half
E
Accuracy
first session
second session
F
P = 0.029
Accuracy
first session
second session

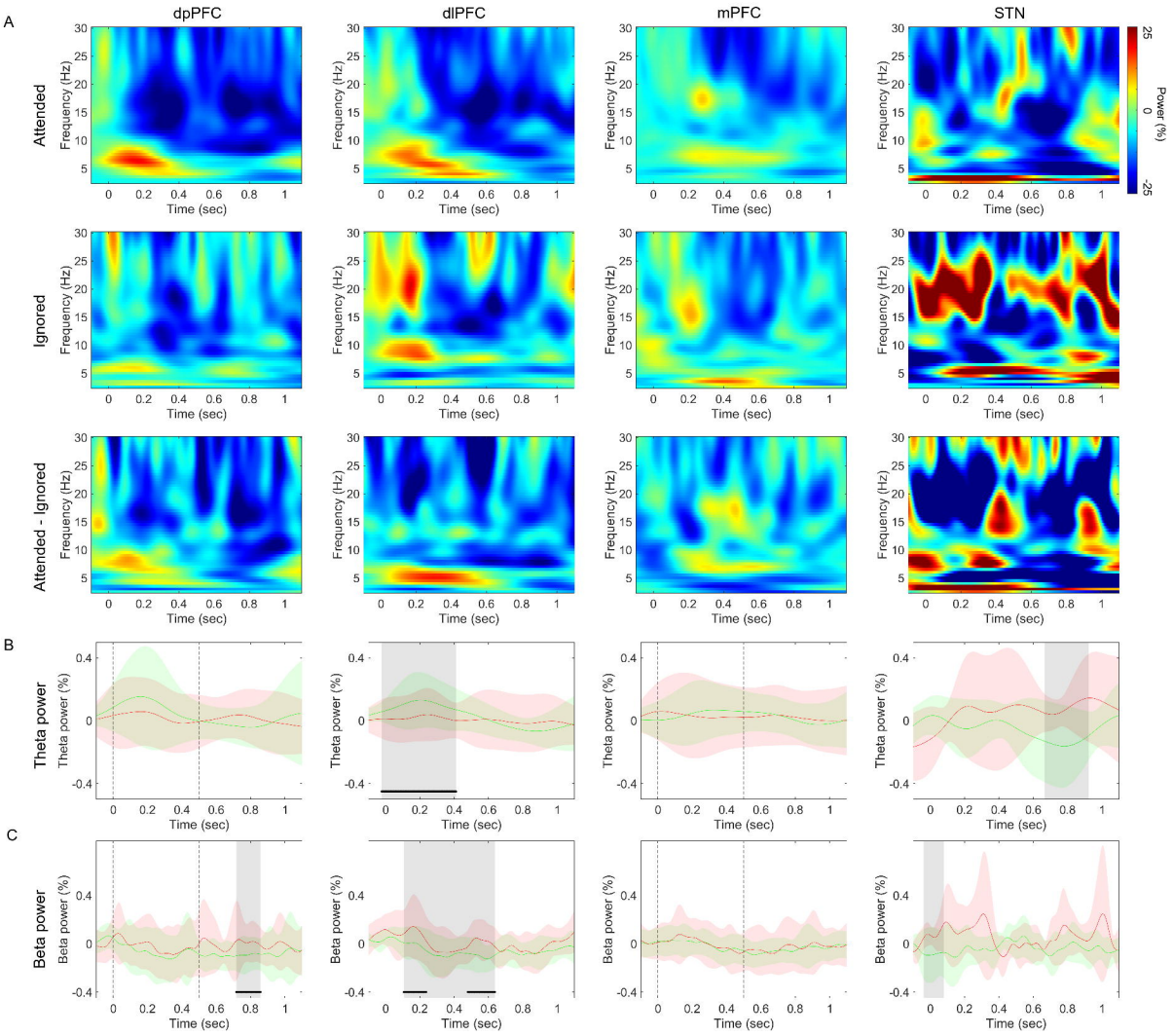
A
dpPFC
dlPFC
mPFC
STN
Attended
Ignored
Attended - Ignored
Frequency (Hz)
Time (sec)
Power (%)
25
0
-25
B
Theta power
Theta power (%)
C
Beta power
Beta power (%)

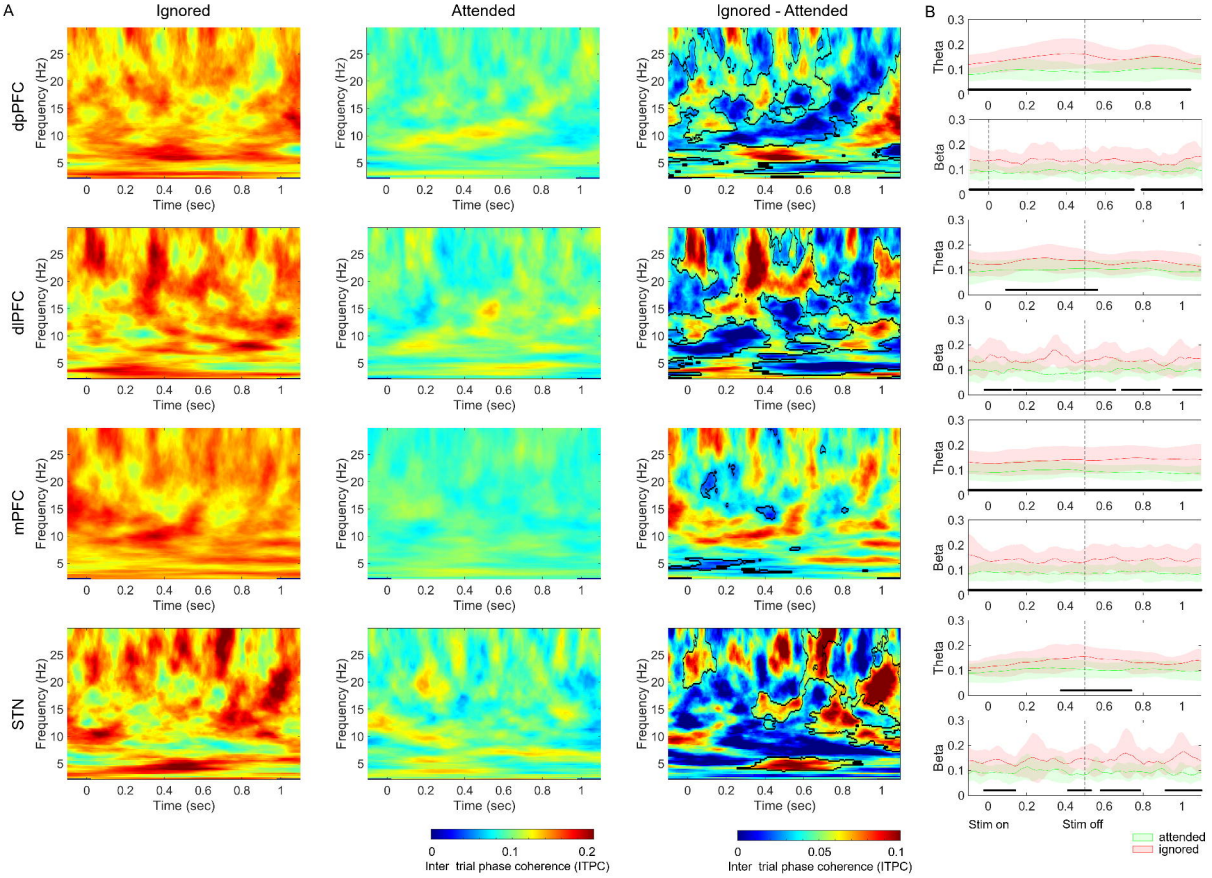
A
Ignored
Attended
Ignored - Attended
dpPFC
dlPFC
mPFC
STN
Frequency (Hz)
Time (sec)
Inter trial phase coherence (ITPC)
B
Theta
Beta
Stim on
Stim off
attended
ignored

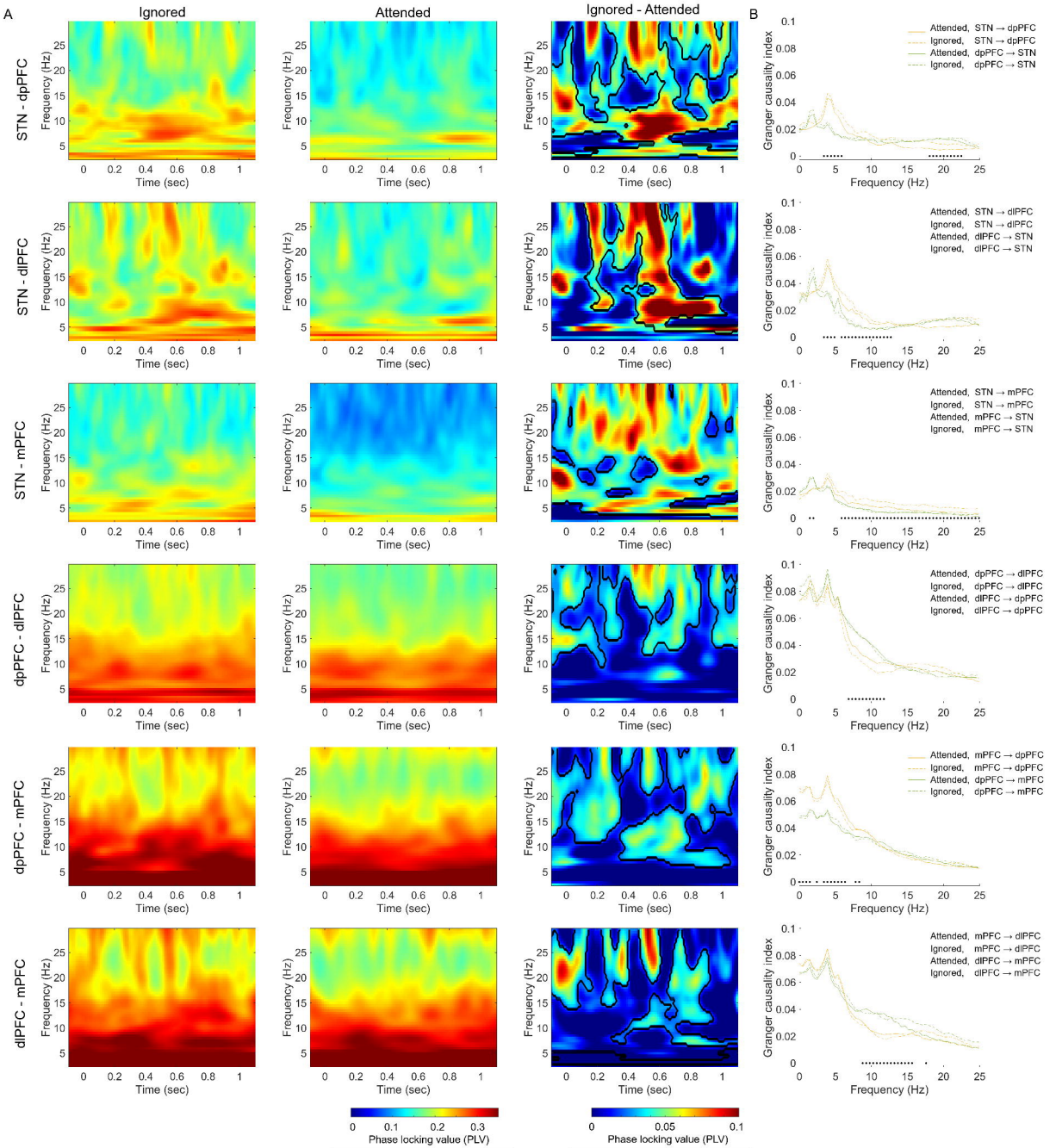
A
Ignored
Attended
Ignored - Attended
B
STN - dpPFC
STN - dlPFC
STN - mPFC
dpPFC - dlPFC
dpPFC - mPFC
dlPFC - mPFC
Frequency (Hz)
Time (sec)
Granger causality index
Attended, STN → dpPFC
Ignored, STN → dpPFC
Attended, dpPFC → STN
Ignored, dpPFC → STN
Attended, STN → dlPFC
Ignored, STN → dlPFC
Attended, dlPFC → STN
Ignored, dlPFC → STN
Attended, STN → mPFC
Ignored, STN → mPFC
Attended, mPFC → STN
Ignored, mPFC → STN
Attended, dpPFC → dlPFC
Ignored, dpPFC → dlPFC
Attended, dlPFC → dpPFC
Ignored, dlPFC → dpPFC
Attended, mPFC → dpPFC
Ignored, mPFC → dpPFC
Attended, dpPFC → mPFC
Ignored, dpPFC → mPFC
Attended, mPFC → dlPFC
Ignored, mPFC → dlPFC
Attended, dlPFC → mPFC
Ignored, dlPFC → mPFC
Phase locking value (PLV)
Phase locking value (PLV)

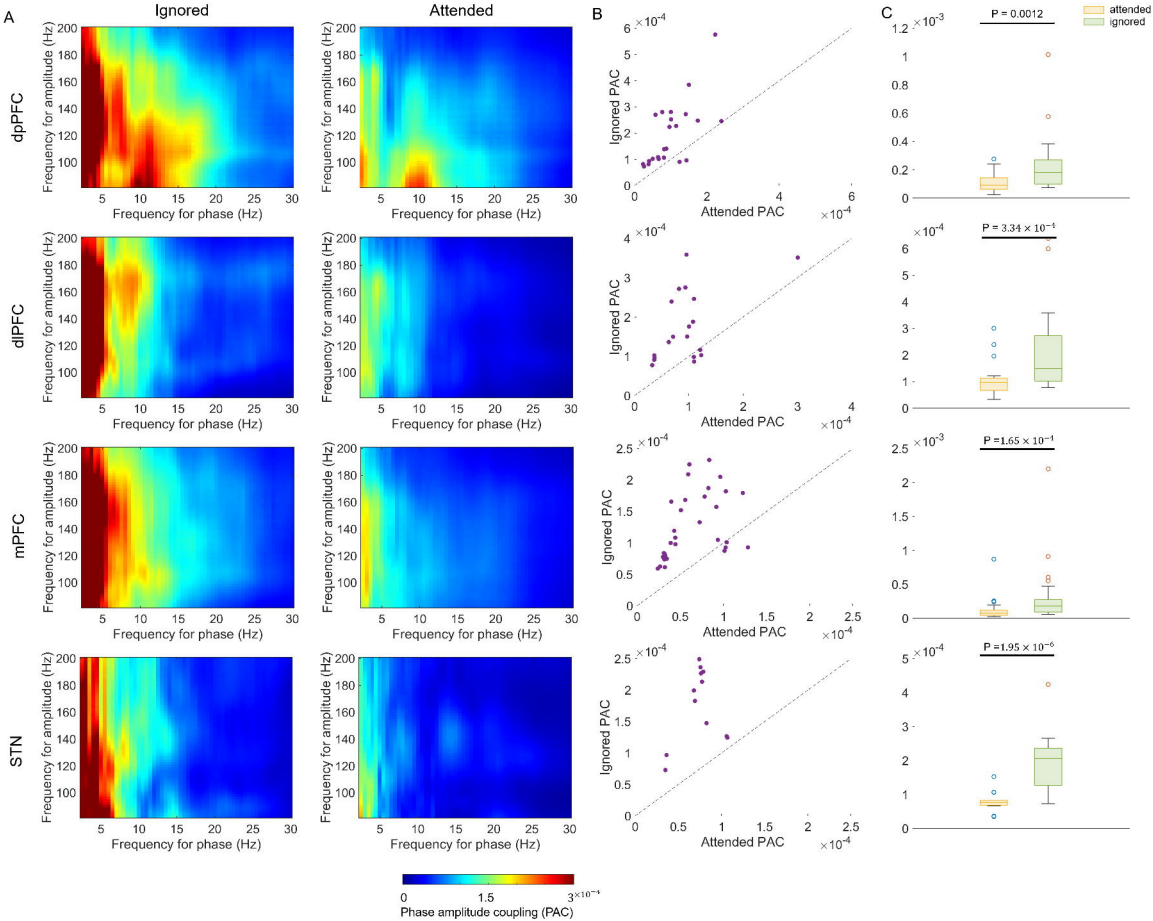
A
Ignored
Attended
dpPFC
dlPFC
mPFC
STN
Frequency for amplitude (Hz)
Frequency for phase (Hz)
B
Ignored PAC
Attended PAC
C
P = 0.0012
P = 3.34 × 10⁻⁴
P = 1.65 × 10⁻⁴
P = 1.95 × 10⁻⁶
attended
ignored
Phase amplitude coupling (PAC)

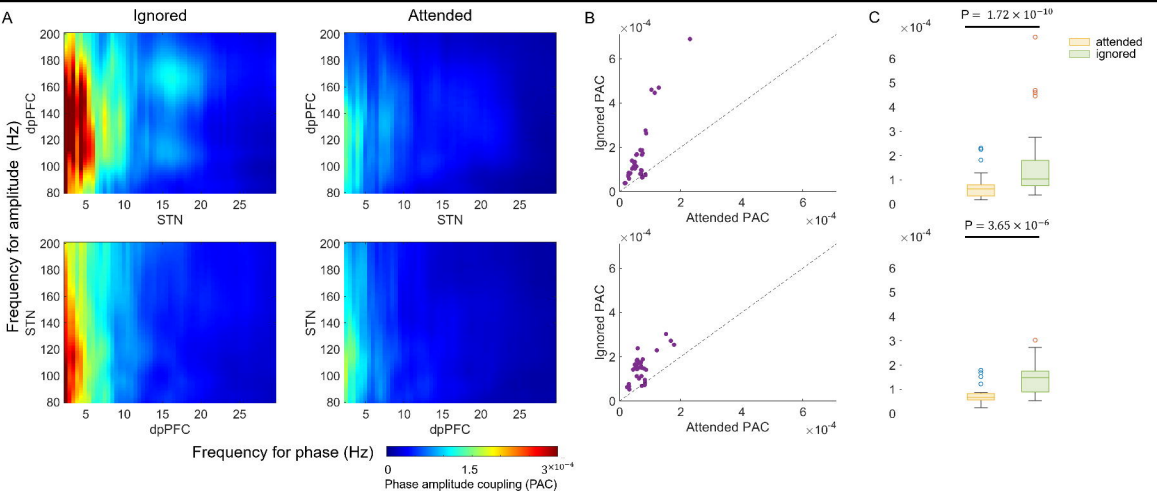
A
Ignored
Attended
Frequency for amplitude (Hz)
dpPFC
STN
Frequency for phase (Hz)
Phase amplitude coupling (PAC)
B
Ignored PAC
Attended PAC
C
P = 1.72 × 10^−10
P = 3.65 × 10^−6
attended
ignored